THE JOURNAL OF PHYSICAL CHEMISTRY B

Article

pubs.acs.org/JPCB

Aggregation Behavior of Rod−Coil−Rod Triblock Copolymers in a Coil-Selective Solvent

Ahmad K. Omar,[†] Ben Hanson,[†] Ryan T. Haws,[‡] Zhongjian Hu,[‡] David A. Vanden Bout,[‡] Peter J. Rossky,[§] and Venkat Ganesan*[,†]

[†]Department of Chemical Engineering and [‡]Department of Chemistry, University of Texas at Austin, Austin, Texas 78712, United States

[§]Department of Chemistry, Rice University, Houston, Texas 77251, United States

ABSTRACT: Recent experiments have reported that the self-assembly of conjugated polymers mimicking rod−coil−rod triblock copolymers (BCPs) in selective solvents exhibits unique aggregate morphologies. However, the nature of the arrangement of the polymers within the aggregates and the spatial organization of the aggregates remain an unresolved issue. We report the results of coarse-grained Langevin dynamics simulations, which investigated the self-assembly behavior of rod−coil−rod BCPs in a coil-selective solvent. We observe a rapid formation of cylindrically shaped multichain clusters. The initial stages of formation of the aggregates was seen to be independent of the strength of the solvent selectivity. However, for higher solvent selectivities, the clusters were seen to merge into larger units at later stages. A reduction in rod to coil block ratio was observed to decrease the size and number of clusters. In the limit of a highly concentrated solution, we observe the formation of a networked system of distinct clusters, which however retain the cylindrical arrangement observed at lower polymer concentrations.

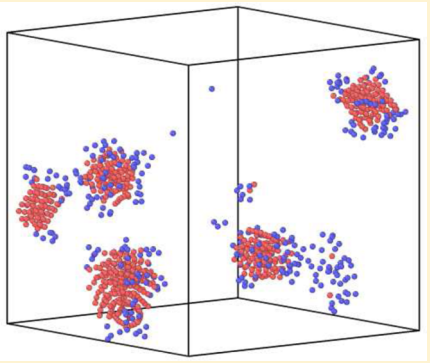

I. INTRODUCTION

The nanostructure of self-assembled block copolymers (BCPs) containing both rigid (rod) and flexible (coil) blocks has been an area of active research. The incorporation of rod blocks into a BCP results in a wide variety of self-assembly behavior arising from the interplay of microphase separation of the rod and coil blocks and the liquid crystalline alignment of rod blocks.[1,2] The present work is specifically motivated by results of recent experiments, which have studied the self-assembly in solution of triblock copolymers containing rod-like blocks. For instance, Huo et al. used fluorescence spectra and UV−vis absorption to characterize the self-assembly of both oligo(*p*-phenyleneethynylene)(OPE)−polystyrene(PS)−oligo(*p*-phenyleneethynylene)(OPE) and PS−OPE−PS in solutions containing varying combinations of toluene and hexane.[3] They characterized the relatively short OPE group as a rod and the longer PS unit as a coil. They found that the triblock copolymers self-assembled into different aggregate structures depending upon the solvent quality (i.e., the affinity of the solvent to the rod block) and the architecture of the copolymer. Similarly, in a recent work, we studied the self-assembly of poly(3-hexylthiophene)-*block*-poly(*tert*-butyl acrylate)-*block*-poly(3-hexylthiophene) (P3HT-*b*-PtBa-*b*-P3HT) triblock (rod−coil−rod) copolymers in solution.[4] We found that as we transitioned to a poor solvent for the P3HT block, the P3HT rod blocks collapse and form aggregates, which exhibited an electronic spectra similar to those observed in P3HT thin films. Such experiments have raised a fundamental interest in the aggregate structures and morphologies of triblock rod−coil copolymers in solution.

Computer simulations have long served as an attractive means to study the morphology of di- and multiblock copolymers in solutions and melts.[5,6] Not surprisingly, a number of studies have considered the self-assembly of rod−coil diblock copolymers in both melts and solution and have presented results characterizing the nanostructures/morphologies in terms of phase diagrams.[1,2,7−11] In contrast, the understanding of the self-assembly and organization of multiblock rod−coil BCPs is comparatively less developed.[3,4,12] Huang et al. performed DPD simulations of rod−coil−rod copolymers in rod-selective solvent and observed the formation of large bowl-like aggregates and, in some cases, spherical vesicles.[13] They later investigated the aggregation behavior in a rod-repulsive solvent and found aggregate formation to be dependent on the compatibility between rod and coil blocks.[14] Using self-consistent-field lattice techniques, Chen et al. observed the formation of spherelike, lamellar, gyroidlike, and cylindrical structures in rod−coil−rod copolymer melts.[15] These structures were only observed for moderate rod fractions such that the enthalpic benefits of rod aggregation were comparable to the coil entropy.

To the best of our knowledge, there has yet to be any simulation or theoretical study on the nature of aggregates that

Received: September 5, 2014
Revised: October 28, 2014
Published: December 16, 2014

result in rod−coil−rod copolymers in coil-selective solvents. A few outstanding questions include: What is the morphology of the resulting aggregate structure and its dependence on the solvent quality? What is the influence of the relative molecular weights of the rod and coil block and the concentration of the copolymers upon the aggregate structure? What is the influence of the architecture of the copolymer, or more explicitly, the differences between rod−coil−rod and coil−rod−coil copolymers, upon the resulting aggregate structure and morphologies?

Motivated by the above considerations, in this Article we report the results of Brownian dynamics simulations of a coarse-grained model used to analyze the self-assembly behavior of rod−coil−rod BCPs in a coil-selective solvent. With our model, we study the effects of solvent selectivity, block architecture, and triblock concentration on the structure of aggregates and the kinetics of formation. The rest of this Article is arranged as follows. In section II, we briefly outline our coarse-grained model and simulation methodology, followed by a discussion of our results in section III. In section IV, we conclude with a summary of our results.

II. SIMULATION DETAILS

Model and Approach. Recently, a number of computer simulations have investigated the structure and morphology of conjugated polymers using different levels of models. Atomistically detailed approaches serve to furnish the most realistic description of the system, but are prohibitively expensive to study the aggregation behavior of multichain systems. Field-theoretic and other coarse-grained approaches have also been widely used for studying self-assembly of rod−coil like copolymers.[7,15−17] Such methods are well suited for studying the equilibrium behavior in concentrated and melt like systems wherein there exists a degree of universality, which is independent of the atomistic details of the polymer. However, such approaches are more cumbersome for solution-based systems, and often do not furnish a straightforward way to characterize the organization of chains within the aggregates. Moreover, methodologies to incorporate kinetics into such a framework are still not well-developed.

As a compromise between the atomistically detailed description and coarse-grained field theoretic approaches, in this work we adopt an intermediate level of description in which we use a bead−spring like micromechanical description within an implicit solvent framework to study the self-assembly of triblock copolymers. Such a level of description has been extensively used in the context of di- and multiblock copolymers to study the self-assembly in both melt-like and solution conditions.[10,18,19] Such methodologies allow for the study of a variety of parameters, such as the concentration of the copolymers, architecture of the chains, solvent quality (modeled implicitly through the effective interactions between the unlike blocks), etc. Moreover, issues such as kinetics of evolution of morphology, the conformation of the chains within the aggregate, etc., can be straightforwardly assessed.[13,18,19]

Our model consists of symmetric triblock copolymers of the form $A_xB_yA_x$, with A and B representing rod and coil monomers, respectively. Unless otherwise mentioned, most of our results pertain to the default architecture corresponding to $A_6B_6A_6$. Our coarse-grained model captures the main physical features of our system, the rigidity of the rod blocks and the selectivity of the solvent toward the coil midblock. Explicitly, a harmonic bond potential is enforced to link all of the chain beads:

$$U_{\text{bond}} = K_b(r - r_0)^2 \tag{1}$$

where K_b represents the spring constant and r_0 represents the equilibrium bond distance. To model the rigidity of the rod blocks, the following bending potential is enforced on the A monomers:

$$U_{\text{angle}} = K_a(\cos(\theta) - \cos(\theta_0))^2 \tag{2}$$

where K_a is the bending rigidity and θ_0 is the equilibrium angle, which is set at 180°. The values of the K_b and K_a were chosen respectively as $6.7 \times 10^4\varepsilon/\sigma^2$ and $8.3 \times 10^3\varepsilon$, while r_0 was chosen to be 1.0σ for A−B and B−B bonds and 0.75σ for A−A bonds. These parameters are similar to those employed by Li et al. in their modeling of coil−rod−coil polymers in solution.[19]

The intermolecular potential between beads was chosen to be a standard shifted and truncated Lennard-Jones (LJ) 6-12 potential of the form:

$$U_{ij}(r) = \begin{cases} 4\varepsilon\left[\left(\frac{\sigma_{ij}}{r}\right)^{12} - \left(\frac{\sigma_{ij}}{r}\right)^{6} - \left(\frac{\sigma_{ij}}{r_{ij}^c}\right)^{12} + \left(\frac{\sigma_{ij}}{r_{ij}^c}\right)^{6}\right], & r \le r_{ij}^c \\ 0, & r > r_{ij}^c \end{cases} \tag{3}$$

For simplicity, σ_{ij} is assumed to be the same (and denoted as σ in this Article) for all pairwise interactions. To mimic the fact that the rod monomers are in a poor solvent, the LJ cutoff distance for rod monomers, r_{AA}^c, is set to 2.5σ, ensuring attractive interactions between rod monomers. Meanwhile, for coil−coil and rod−coil interactions, we truncate and shift the LJ potential at a cutoff distance of $2^{1/6}\sigma$ so that these pairs only experience repulsive interactions. The depth of the LJ potential well is fixed at ε for rod−coil and coil−coil interactions. However, for interactions between A monomers, the depth of well, ε_{AA}, is a key parameter of interest as it implicitly represents the selectivity of the solvent, and hence we study different values. The default value of ε_{AA} is set to a value of 2ε unless stated otherwise. We present our results in reduced units in which $\sigma = \varepsilon = m = 1$ with τ the unit of time defined as $\tau = (\sigma^2/(m\varepsilon))^{1/2}$.

We model the dynamics of the system in an implicit solvent framework using a Langevin dynamics simulation approach. In such a framework, the equation of motion for bead i is

$$m_i\frac{d^2\vec{r}_i}{dt^2} = -\nabla(U_i^b + U_i^{nb}) - \mu\frac{d\vec{r}_i}{dt} + \vec{f}_i(t) \tag{4}$$

In the above, $\vec{r}_i$ denotes the position of the bead i, and U_i^b and U_i^{nb}, respectively, represent the sums of all of the bonded and nonbonded interaction potentials experience by the bead i. Moreover, μ denotes the friction coefficient for the Langevin dynamics, and $\vec{f}_i(t)$ represents the random forces of solvent particles and is related to μ (taken to be 30.0) by the fluctuation dissipation theorem $\langle\vec{f}_i(t)\vec{f}_j(t')\rangle = 2\mu k_B T\delta_{ij}\delta(t - t')\mathbf{I}$, where $\mathbf{I}$ is the unit tensor. All simulations were performed in a cubic cell of length 30.0 with periodic boundary conditions.

To ensure that the aggregation characteristics are independent of the box size, we performed simulations at equal volume fractions with several different box sizes while starting from differing random initial conditions. Moreover, to further ensure that our morphologies are not artifacts of our random initial conditions, we also implemented the molecular dynamics replica exchange method used by Sugita and Okamoto.[20] The

dx.doi.org/10.1021/jp509016c | J. Phys. Chem. B 2015, 119, 330−337

upper bound for our temperature series were temperatures at which rod monomer associations were reversible, while our lower bound in the series consisted of our temperature of interest, $k_BT = 2$, where strong aggregation did occur. We took care to choose a temperature series that allowed for the reported optimum exchange rate between replicas of around 20%.[21] A geometric temperature series of the form $T_i = T_0\, e^{ki}$ was found to provide these optimum exchange rates for nearly all of the replicas, where k is a constant found by iteration to provide the desired exchange rate, T_0 is the temperature of interest, and T_i is the temperature of replica i. Initially, the chains in each replica were randomly configured within the cubic cell with all bond and angles at the appropriate equilibrium values. Each replica was then equilibrated through dynamic simulation using an integration time step $\Delta t = 7 \times 10^{-4}$ for a duration of 2×10^7 cycles before replica swaps were attempted. Configurations at our temperature of interest, which originated from higher temperatures in the series, were then equilibrated for an additional 1.0×10^8 cycles. The resulting morphologies were found to be consistent with those of systems initialized from random configurations. Unless otherwise stated, all data reported are taken by averaging 16 independent samples run for a duration of 1.2×10^8 cycles. All simulations were performed utilizing the MD simulation package LAMMPS.[22]

Cluster Analysis. To characterize the self-assembly behavior of these polymers, we used a methodology for defining clusters, which is based on a connectivity matrix algorithm.[23−25] Typically, the component of interest in these triblock copolymers are the self-assembling rods (i.e., the photoactive layer in PtBa-P3HT triblocks), and hence we use the latter to define the clusters. Rod monomers within a cutoff distance of 2.0 of each other are grouped into the same cluster. If all of the rod monomers for a given chain are in a single cluster, the coil monomers for that chain are also assigned to be within that cluster. If, instead, the rod monomers span two different clusters, this indicates that the coil block of that chain joins two clusters (a cross-link, denoted in this Article as X_L), and we then do not count the coil monomers for either cluster. To ensure that at least two chains are participating in our clusters, we omit any aggregates with less than three rod blocks from our discussion. Using this analysis, we identify the following characteristics of the morphology of the system: (i) the total number of clusters, N_{cl}; (ii) the average number of beads per cluster (i.e., aggregation number) normalized by the chain degree of polymerization, N_{Ag}; (iii) the average radius of gyration of the clusters, R_g^2, where the radius of gyration of a cluster containing n beads is given as

$$R_{g,cl}^2 = \frac{1}{n}\sum_{i=1}^{n}(r_i - r_{com})^2 \tag{5}$$

where r_i and r_{com} are the coordinates of bead i and the cluster center of mass, respectively; and (iv) the average number of rod blocks per cluster normalized by the number of total system rod blocks, f_{rod}, which proves to be a useful parameter in quantifying the presence of extremely large aggregates or comparing average aggregate sizes among systems of varying size. Furthermore, we compute the radial distribution function between the rod blocks center of mass, defined as

$$g(r) = \frac{V}{4\pi r^2 N_{rod}^2}\left\langle \sum_i \sum_{j\neq i} \delta(r - r_{ij}) \right\rangle \tag{6}$$

where N_{rod} is the number of rod blocks, and r_{ij} is the distance between the center of mass of rod i with that of rod j.

In the following section, we initially focus our discussions on relatively dilute solutions with a volume fraction (defined as $\phi_c = \pi\sum\sigma_i^3/(6V)$) of $\phi_c = 0.017$. In this dilute regime, we explore the time evolution of aggregation and the nature of the resulting structures. The effects of increasing solvent selectivity, ε_{AA}, and varying the relative rod to coil block lengths on the aggregation is also reported. Subsequently, we discuss the effects of increasing ϕ_c on the structure of the aggregates.

III. RESULTS AND DISCUSSION

Aggregate Morphology and Time Evolution. Figure 1a displays a typical equilibrium configuration of our system in the dilute regime. We observe the self-assembly of the rod blocks into cylindrically shaped clusters each comprised of multiple chains with the rod blocks aligned in a parallel fashion. The nature of these aggregates is in agreement with the experimental findings of Huo et al., wherein they hypothesized the formation of cylindrically shaped aggregates containing multiple chains with a core of parallel rod blocks.[3] In some instances, the cylindrical aggregates were seen to merge and form a larger string-like aggregate (Figure 1b). However, among the configurations sampled for the default parameters and time scales observed, the latter kinds of morphologies were found to be rare due to the entropic limitations and the kinetics associated with the merging of aggregates. The propensity to form these large aggregates as a function of solvent selectivity is examined later in this Article.

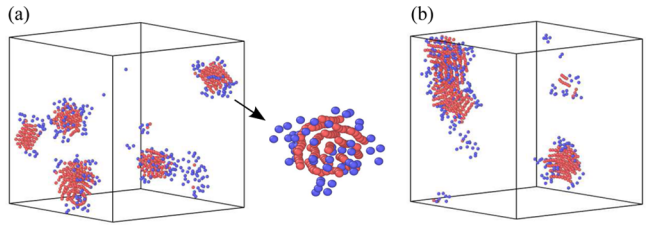

Figure 1. Snapshots of equilibrium conformation of $\phi_c = 0.017$ (50 chains) system. (a) Common system configuration consisting of several cylindrical aggregates. A snapshot of the axis of symmetry of one of the clusters is also shown. (b) Configuration in which the cylindrical clusters were found to merge to form a larger string-like aggregate. Red and blue beads represent rod and coil monomers, respectively.

The time evolution of the morphologies is quantified in Figure 2a and b through the number of clusters N_{cl} and the radial distribution function. It can be seen that broadly aggregation occurs as a two-step process: an initial stage (magnified for clarity in the inset of Figure 2a) in which the number of clusters rapidly increases accompanied by a significant decrease in the system energy (see inset of Figure 2b). In this stage, enthalpic considerations are expected to be dominant, and the system aggregates in such a manner that the spatially accessible rod monomers organize together into clusters. However, such a process is expected to lead to a number of entropically unfavorable configurations and misalignments, and hence is seen to be followed by a slower,

dx.doi.org/10.1021/jp509016c | J. Phys. Chem. B 2015, 119, 330−337

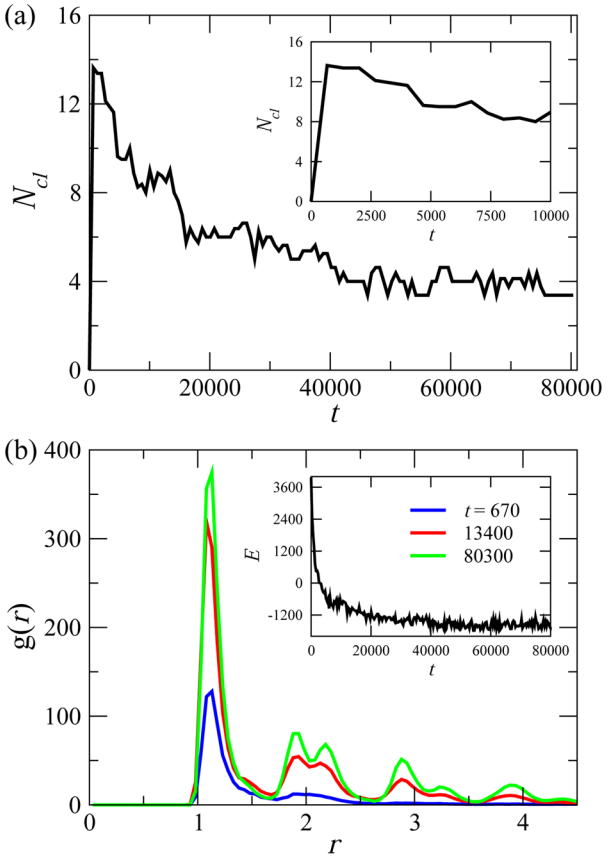

Figure 2. (a) Number of clusters as a function of time (the inset depicts the initial stages of self-assembly). (b) Corresponding center of mass of A block RDF's at various simulation times. Note that the peaks are spaced at a distance ratio equivalent to that of hexagonal packing ($1:\sqrt{3}:2:\sqrt{7}$). The inset displays a typical system energy as a function of time.

second stage of rearrangement, during which a few of the clusters are seen to combine leading to a drop in the number of clusters.

The nature of the ordering within the clusters is displayed in Figure 2b through the rod block center of mass radial distribution functions and supports the picture presented above. It is seen that the initial stages are accompanied by the emergence of an aggregate without well-defined internal packing of the rod monomers (as seen in the lack of clear higher order peaks). Subsequently, there is seen to be formation of more tightly packed aggregates, which exhibit clear higher order peaks. The ratio of the distance between peaks is seen to be consistent with hexagonal packing of the rods, a result that was also observed in simulations of coil–rod–coil chains.[19]

Interestingly, the rod constituents of the string-like aggregates are stacked perpendicularly to the long axis of the aggregate (see Figure 1b), and resemble amyloid fibrils seen in β-sheet stacked proteins.[26] Indeed, it has been shown through experiments and atomistic MD simulations that fibrils resembling those formed by natural proteins can be made through the aggregation of short aliphatic peptide sequences.[27,28] Our results above suggest a tantalizing hypothesis that the formation of such fibril-like structures is more likely tied to the rigidity of the backbone units and their degree of interactions with the solvent rather than the specific sequence of the protein themselves.

Role of Solvent Selectivity. Experiments have suggested that the aggregate morphologies of rod–coil BCPs in solution depend sensitively on the degree of solvent selectivity toward the different blocks.[1,3,29] A parameter of specific interest in this work is the solvophobicity of the rod blocks and its influence upon the aggregate morphologies.

In Figure 3a and b, we display the influence of ε_{AA} upon the number of clusters (with the initial stages more explicitly

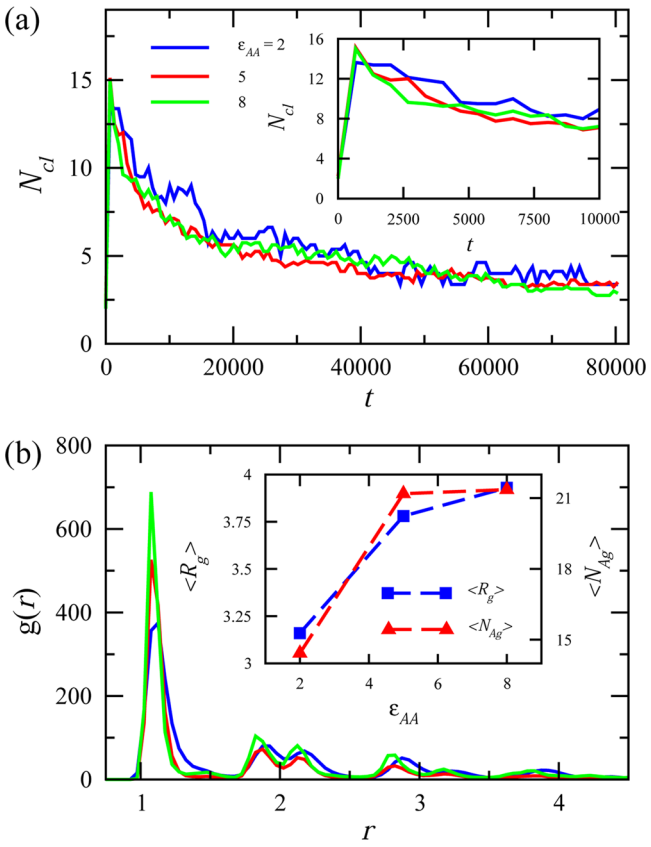

Figure 3. Effects of segregation strength on (a) the number of clusters as a function of time (the inset depicts the initial stages of self-assembly); and (b) the center of mass of A block RDF's (the inset displays the corresponding average radius of gyration and aggregation number of the clusters).

displayed in the inset of Figure 3a) and the radial distribution functions of the rod blocks. The average radius of gyration of the cluster and the aggregation numbers are displayed in the inset of Figure 3b. From Figure 3a, we observe that the initial stages of aggregate formation are not very sensitive to the solvent selectivity, and result in approximately the same number of clusters. This is consistent with the picture discussed above in which the initial stages of aggregation were suggested to be driven by the spatial proximity of the rod monomers. The influence of solvent selectivity is however seen to clearly manifest in the later stages of cluster evolution and results in a smaller number of clusters for larger ε_{AA}. Such a result is also seen to be reflected in the larger average cluster aggregation number and radius of gyration shown in Figure 3b. This increase in aggregate size can be understood to be a consequence of increased enthalpic benefits of the rod interactions in poorer solvents, which outweigh the conforma-

dx.doi.org/10.1021/jp509016c | J. Phys. Chem. B 2015, 119, 330–337

tional entropy losses of the coil blocks. The latter results are consistent with the experimental findings of Huo et al. wherein a reduction of the conformational entropy of the coil block through solvent quality led to the formation of larger aggregate structures.[3]

In Figure 3b, we depict the influence of ε_{AA} upon the radial distribution functions of the rod blocks within the clusters. We observe that with an increase in ε_{AA}, the first coordination shell of the RDF is enhanced, which is indicative of increased propensity for aggregation of the rods. Interestingly, as is evident from the location of the peaks in $g(r)$, the overall hexagonal packing of the aggregates is seen to be retained even at the highest ε_{AA}. These results suggest that the solvent selectivity has only an influence on the size of the clusters and not on the morphology of packing of the rods within the cluster.

As discussed earlier, some of our simulation results were found to result in morphologies in which several clusters merge such that the system contains very large string-like aggregates. These types of aggregates were consistently found when any one cluster comprised 60% or more of the total system rod blocks. To quantify the propensity for formation of such aggregates, we used the measure f_{rod}, which quantifies the average number of rod blocks per cluster normalized by the total number of rod blocks in the system. Figure 4a illustrates the probability distribution of the cluster rod fractions, $P(f_{rod})$, for different solvent selectivities. The corresponding probability distribution of the radius of gyration, $P(R_g)$, is displayed in Figure 4b. Clearly, with increasing solvent selectivity, the probability of forming larger aggregates is seen to increase,

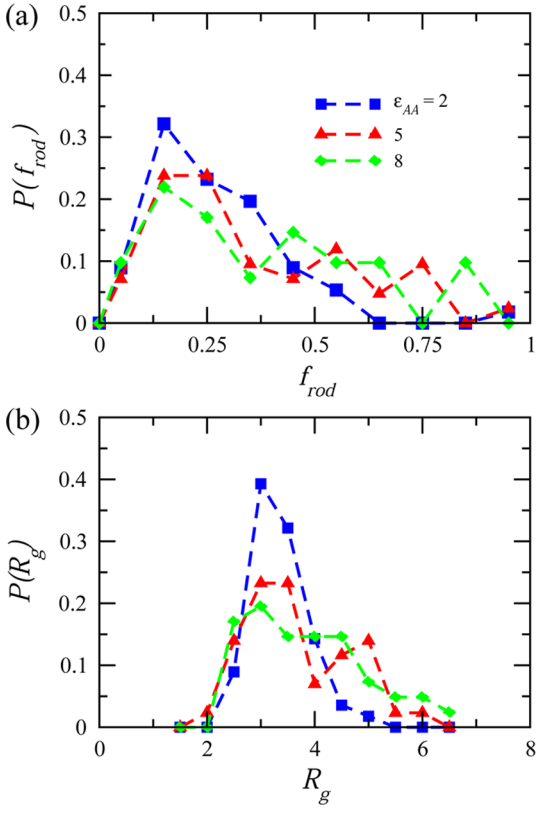

Figure 4. Effects of segregation strength on (b) the rod fraction probability distribution; and (b) the probability distribution of the radius of gyration of clusters.

resulting in some cases in which the f_{rod} is close to 0.75. However, even for higher values of ε_{AA}, the dominant morphology is still seen to be that of several cylindrical clusters, as indicated by the peak of the distribution remaining around f_{rod} = 0.13.

The above results suggest that rendering the solvent poorer for the rod block results in an increased propensity to form larger clusters. Interestingly, however, the peak in the cluster size distributions is seen to be independent of the solvent selectivity for the rod blocks. Moreover, the clusters are seen to maintain the cylindrical shape and hexagonally packed arrangements at all solvent selectivities.

Influence of Block Architecture. We expect that the enthalpic and entropic forces underlying cluster formation would be modulated by changes in the block architecture (i.e., rod to coil block length ratio, x/y). Figure 5 summarizes our

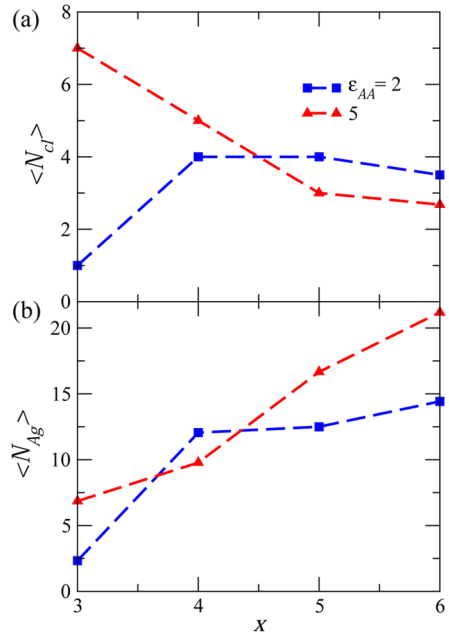

Figure 5. (a) Number of clusters and (b) average cluster aggregation number as a function of block rod block length and segregation strength for symmetric polymer chains $A_xB_yA_x$ with a fixed total number of monomers ($2x + y = 18$). For these results, initial conditions were held constant between runs of identical block architecture.

results for the cluster characteristics upon varying the rod block length (the total number of beads is fixed). Interestingly, from the radial distribution functions displayed in Figure 6, we observe that for all rod lengths, the aggregates maintain the same hexagonal packing discussed in earlier sections. For relatively large segregation strengths (ε_{AA} = 5), the dominant free energy contribution is the aggregation of the rod blocks. Driven by such enthalpic contributions, the number of clusters (aggregation number) is seen to monotonically decrease (increase) with increasing rod length. However, at lower segregation strengths, we observe that the number of clusters exhibits a nonmonotonic trend with respect to the rod block length. We reason that this trend arises from a crossover in which the enthalpic driving force for cluster−cluster interactions outweighs the accompanying entropic penalty. Explicitly, at lower segregation strengths (ε_{AA} = 2), one would expect the entropy of the coil blocks to play a larger role in

dx.doi.org/10.1021/jp509016c | J. Phys. Chem. B 2015, 119, 330−337

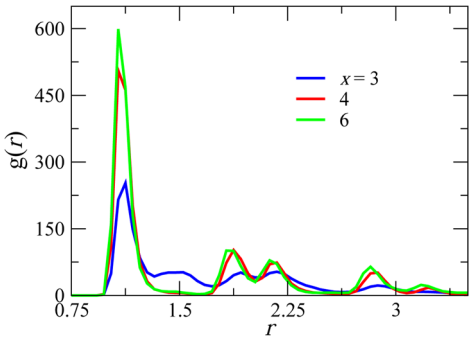

Figure 6. Center of mass of A block RDF's for ε_{AA} = 5 for various rod lengths.

aggregate formation. Consistent with such expectations, when x = 3 (corresponding to small rod lengths), only one small cluster is observed to form with the rest of the system comprised of individual chains. This is in accord with the findings of Huo et al. wherein, at short rod lengths, they found little interchain aggregation.[3] For these short rod lengths, they observed that the formation of larger cylindrical aggregates was induced due to the reduction in the conformational entropy of the coil block (through decreasing the coil solvent quality), in agreement with our findings.

When the rod length is increased to x = 4, the number of clusters increases with an accompanying increase in the average cluster aggregation number. This initial increase comes as the enthalpic contribution arising from the rod associations becomes comparable to entropy costs incurred by the coil in forming the clusters. Upon further increasing the rod block length, the clusters begin to decrease in number and increase in size. These results are in broad agreement with our previous experimental findings in which we found that decreasing the rod length requires an accompanying decrease in the rod solvent quality to induce aggregation.[4]

Overall, the above results suggest that, while the overall packing and organization of clusters are not affected by the rod to coil block ratios, the number and aggregation number of the clusters show a strong dependency on the latter.

Effects of Polymer Concentration. In Figures 7 and 8, we display the cluster characteristics as a function of the polymer concentration in solution. As may be expected, the number of clusters and the cluster size increase with an increase in the concentration of BCPs (Figure 7a). Furthermore, the snapshot (Figure 8) and the rod block RDF's (shown in Figure 7b) demonstrate that the clusters continue to retain the same cylindrical, hexagonally packed architecture observed at low concentrations.

A distinct feature of the clusters resulting in higher concentrations however is that seemingly distinct clusters are now "linked" through chains that contain the rod blocks in multiple clusters. Such a characteristic is explicitly quantified by the number of cross-links, X_L, displayed in Figure 7c. For dilute concentrations, we observe that the probability of two clusters sharing a chain is almost negligible. However, with increase in

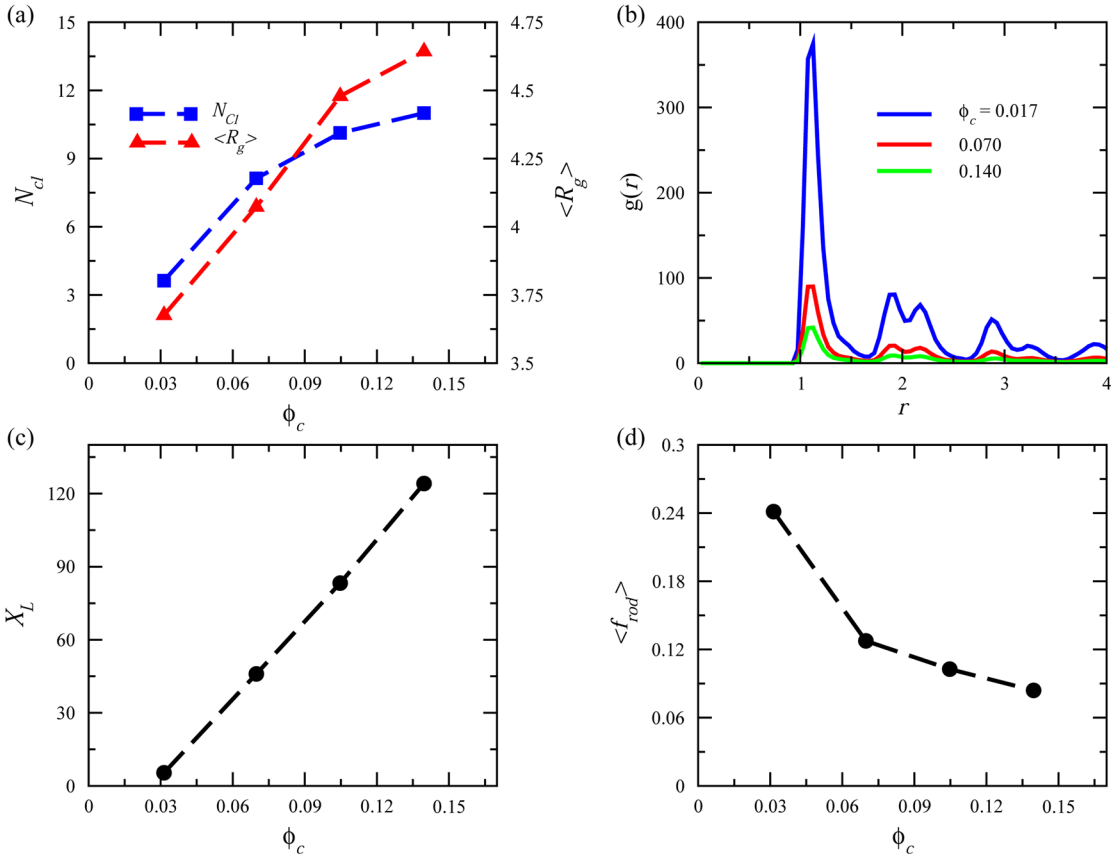

Figure 7. Concentration dependence of (a) the average cluster radius of gyration and number of clusters; (b) the center of mass of A block RDF; (c) the total number of cross-links between clusters; and (d) the average fraction of rods per cluster. Results are the average of eight independent samples for ε_{AA} = 2.

dx.doi.org/10.1021/jp509016c | J. Phys. Chem. B 2015, 119, 330−337

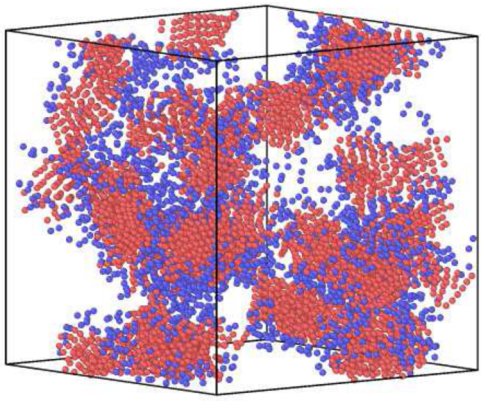

Figure 8. Snapshot of 400 chain system (ϕ_c = 0.14). Red and blue beads represent rod and coil monomers, respectively.

polymer concentration, we observe that the number of cross-links increases nearly monotonically with the volume fraction. These cross-links provide a large energetic and kinetic barrier for adjacent clusters to merge and form the string-like morphologies noted for dilute concentrations. Such an expectation is confirmed by the distinct clusters noted in Figure 8 and is also confirmed by observing the decrease in the average cluster rod fraction $\langle f_{rod} \rangle$ with increasing concentration (Figure 7d).

IV. CONCLUSION

In summary, we presented results from a coarse-grained Brownian dynamics simulation approach to shed insight into the self-assembly of rod−coil−rod BCPs in a coil-selective solvent. We considered the influence of polymer selectivity, rod to coil length ratios, and polymer concentration upon characteristics of clusters resulting in such systems. Our simulations indicated the formation of a cylindrically shaped cluster in agreement with experimental observations (and the corresponding results for coil−rod−coil BCPs). The initial stages of cluster formation were observed to result in aggregates that were independent of the segregation strength. Increasing the solvent selectivity toward the coil was observed to provide a driving force for neighboring clusters to merge. Furthermore, increasing the segregation strength was found to significantly increase the probability of forming large string-like aggregates. As the polymer concentration was increased, the clusters began to form a cross-linked network while retaining their overall cylindrical character.

In comparing our results to those reported in simulations for coil−rod−coil BCPs,[19] we observe that rod−coil−rod exhibits similar structures (we note that Li et al. did not report cluster characteristics) at segregation strengths that are comparatively lower. However, in contrast to the situation for coil−rod−coil BCPs, we did not see structures possessing long-range order (such as the disk morphologies reported by Li et al.) despite increasing the segregation strength to several k_BT. We reason that this is due to the increased entropic penalty associated with a middle coil block versus the end coil blocks in forming these types of structures. These results suggest that the architecture of the block copolymer plays a significant role in influencing the morphology of the organization in such systems.

AUTHOR INFORMATION

Corresponding Author

*E-mail: venkat@che.utexas.edu.

Notes

The authors declare no competing financial interest.

ACKNOWLEDGMENTS

This material is based upon work supported as part of the program Understanding Charge Separation and Transfer at Interfaces in Energy Materials (EFRC:CST), an Energy Frontier Research Center funded by the U.S. Department of Energy (DOE), Office of Science, Office of Basic Energy Sciences (BES), under Award no. DE-SC0001091. We acknowledge the Texas Advanced Computing Center (TACC) at The University of Texas at Austin for providing computing resources that have contributed to the research results reported within this Article. V.G. acknowledges partial support by a grant from the Robert A. Welch Foundation (Grant F1599).

REFERENCES

(1) Olsen, B. D.; Segalman, R. A. Self-assembly of rod-coil block copolymers. *Mater. Sci. Eng., R* **2008**, *62*, 37−66.

(2) Zhang, J.; Chen, X.-F.; Wei, H.-B.; Wan, X.-H. Tunable assembly of amphiphilic rod-coil block copolymers in solution. *Chem. Soc. Rev.* **2013**, *42*, 9127−9154.

(3) Huo, H.; Li, K.; Wang, Q.; Wu, C. Self-assembly and optical property of triblock copolymers made of polystyrene and oligo(p-phenyleneethynylene) in different mixtures of toluene and hexane. *Macromolecules* **2007**, *40*, 6692−6698.

(4) Brazard, J.; Ono, R. J.; Bielawski, C. W.; Barbara, P. F.; Vanden Bout, D. A. Mimicking conjugated polymer thin-film photophysics with a well-defined triblock copolymer in solution. *J. Phys. Chem. B* **2013**, *117*, 4170−4176.

(5) Gavrilov, A. A.; Kudryavtsev, Y. V.; Chertovich, A. V. Phase diagrams of block copolymer melts by dissipative particle dynamics simulations. *J. Chem. Phys.* **2013**, *139*, 224901.

(6) Groot, R. D.; Madden, T. J. Dynamic simulation of diblock copolymer microphase separation. *J. Chem. Phys.* **1998**, *108*, 8713.

(7) Pryamitsyn, V.; Ganesan, V. Self-assembly of rod-coil block copolymers. *J. Chem. Phys.* **2004**, *120*, 5824−5838.

(8) Kumar, N. A.; Ganesan, V. Communication: Self-assembly of semiflexible-flexible block copolymers. *J. Chem. Phys.* **2012**, *136*, 101101.

(9) Shah, M.; Pryarnitsyn, V.; Ganesan, V. A model for self-assembly in side chain liquid crystalline block copolymers. *Macromolecules* **2008**, *41*, 218−229.

(10) Horsch, M. A.; Zhang, Z.; Glotzer, S. C. Self-assembly of polymer-tethered nanorods. *Phys. Rev. Lett.* **2005**, *95*, 056105.

(11) Li, K.; Wang, Q. Multiple self-assembled nanostructures from an oligo(p-phenyleneethynylene) containing rod-coil-rod triblock copolymer. *Chem. Commun.* **2005**, 4786−4788.

(12) Chen, X. L.; Jenekhe, S. A. Supramolecular self-assembly of three-dimensional nanostructures and microstructures: Microcapsules from electroactive and photoactive rodcoilrod triblock copolymers. *Macromolecules* **2000**, *33*, 4610−4612.

(13) Huang, J.-H.; Fan, Z.-X.; Ma, Z.-X. Dissipative particle dynamics simulations on self-assembly of rod-coil-rod triblock copolymers in a rod-selective solvent. *J. Chem. Phys.* **2013**, *139*, 064905.

(14) Fan, Z.-X.; Huang, J.-H. Dissipative particle dynamics simulation on aggregation of rod-coil-rod triblock copolymer in dilute solution. *Acta. Phys.-Chim. Sin.* **2014**, *30*, 408−412.

(15) Chen, J.-Z.; Sun, Z.-Y.; Zhang, C.-X.; An, L.-J.; Tong, Z. Self-assembly of rod-coil-rod ABA-type triblock copolymers. *J. Chem. Phys.* **2008**, *128*, 074904.

(16) Drolet, F.; Fredrickson, G. H. Combinatorial screening of complex block copolymer assembly with self-consistent field theory. *Phys. Rev. Lett.* **1999**, *83*, 4317−4320.
(17) Matsen, M. W.; Barrett, C. Liquid-crystalline behavior of rod-coil diblock copolymers. *J. Chem. Phys.* **1998**, *109*, 4108.
(18) Lin, S.; Numasawa, N.; Nose, T.; Lin, J. Brownian molecular dynamics simulation on self-assembly behavior of rod-coil diblock copolymers. *Macromolecules* **2007**, *40*, 1684−1692.
(19) Li, Y.; Lin, S.; He, X.; Lin, J.; Jiang, T. Self-assembly behavior of ABA coil-rod-coil triblock copolymers: A Brownian dynamics simulation approach. *J. Chem. Phys.* **2011**, *135*, 014102.
(20) Sugita, Y.; Okamoto, Y. Replica-exchange molecular dynamics method for protein folding. *Chem. Phys. Lett.* **1999**, *314*, 141−151.
(21) Rathore, N.; Chopra, M.; de Pablo, J. J. Optimal allocation of replicas in parallel tempering simulations. *J. Chem. Phys.* **2005**, *122*, 024111.
(22) Plimpton, S. Fast parallel algorithms for short-range molecular dynamics. *J. Comput. Phys.* **1995**, *117*, 1−19.
(23) Sevick, E. M.; Monson, P. A.; Ottino, J. M. Monte Carlo calculations of cluster statistics in continuum models of composite morphology. *J. Chem. Phys.* **1988**, *88*, 1198−1206.
(24) Surve, M.; Pryamitsyn, V.; Ganesan, V. Universality in structure and elasticity of polymer-nanoparticle gels. *Phys. Rev. Lett.* **2006**, *96*, 177805.
(25) Surve, M.; Pryamitsyn, V.; Ganesan, V. Polymer-bridged gels of nanoparticles in solutions of adsorbing polymers. *J. Chem. Phys.* **2006**, *125*, 064903.
(26) Rambaran, R. N.; Serpell, L. C. Amyloid fibrils: Abnormal protein assembly. *Prion* **2008**, *2*, 112−117.
(27) Lakshmanan, A.; Cheong, D. W.; Accardo, A.; Di Fabrizio, E.; Riekel, C.; Hauser, C. A. E. Aliphatic peptides show similar self-assembly to amyloid core sequences, challenging the importance of aromatic interactions in amyloidosis. *Proc. Natl. Acad. Sci. U.S.A.* **2013**, *110*, 519−524.
(28) Nguyen, H. D.; Hall, C. K. Molecular dynamics simulations of spontaneous fibril formation by random-coil peptides. *Proc. Natl. Acad. Sci. U.S.A.* **2004**, *101*, 16180−16185.
(29) Tu, Y.; Wan, X.; Zhang, D.; Zhou, Q.; Wu, C. Self-assembled nanostructure of a novel coil-rod diblock copolymer in dilute solution. *J. Am. Chem. Soc.* **2000**, *122*, 10201−10205.